Available online at www.sciencedirect.com
ScienceDirect
European Journal of Operational Research 195 (2009) 519–527
EUROPEAN JOURNAL OF OPERATIONAL RESEARCH
www.elsevier.com/locate/ejor

O.R. Applications

Optimization of a one dimensional hypertelescope for a direct imaging in astronomy

Paul Armand [a,*], Joël Benoist [a], Elsa Bousquet [a], Laurent Delage [b], Serge Olivier [b], François Reynaud [b]

[a] XLIM UMR 6172, Département Maths Informatique, Programme Transverse IRO, CNRS et Université de Limoges, France
[b] XLIM, Département Photonique, Programme Transverse IRO, France

Received 16 May 2007; accepted 1 February 2008
Available online 9 February 2008

Abstract

We describe an application of nonlinear optimization in interferometric optical astronomy. The aim is to find the relative positions of the output pupils and the modulus of the beams through each pupil of a linear array of telescopes in order to design an instrument capable of imaging exoplanets. The problem is modelized under the form of a semi-infinite nonlinear minimization problem. The model problem is transformed by a simple discretization into a minimization problem with a finite number of constraints, then it is solved by using a minimization solver. Numerical experiments are reported.

Keywords: Nonlinear programming; Constrained optimization; High contrast imaging; Exoplanet; Hypertelescope; Astronomical technique; Optical systems

1. Introduction

The new generation of high resolution optical imaging system for astronomy is based on the linkage of a telescope array in order to reach micro or nanoradian resolution [6]. The principle of the image restoration uses an indirect method. The interferometric signals give partial information on the spectrum of the object spatial distribution. A numerical image reconstruction is necessary to post-process the data. The usage of this technique never allows to select the light of one pixel in the observed field, for example in order to achieve a direct spectral analysis. The hypertelescope concepts proposed by Labeyrie [4], Vakili et al. [9] and Reynaud–Delage [8] (see also the recent book [5]), answer this problem. By using a specific conditioning of the beam coming from the telescopes, it is possible to perform a direct imaging, thanks to an accurate equalisation of the optical paths and a pupil densification, see Fig. 1.

The first operation, the so called cophasing, has to be achieved with a sub-micrometric accuracy. Overall, in this process, coherent properties of the beams have to be preserved taking care of polarization and dispersion differential effects. The pupil densification is a specific step of the hypertelescope design. The input pupil mapping is homothetically reduced and the resulting beams are expended in order to maximize the densified pupil coverage. The goal of such instruments is to design an optical instrument with a strong dynamic in the frame of a high resolution imaging. For example, the angular separation between a star and an exoplanet is expected to be in the range of nanoradian and the ratio of their intensities can be less than 10^{-6}. Of course, this tremendous result will be reached in a limited field and the number of pixels remains low as reported in [4,8,9].

In a general way, the optimization of optical instrument is addressed in various domains such as microscopy, see for example [7].

* Corresponding author. Tel.: +33 5 55 45 73 30; fax: +33 5 55 45 73 22.
E-mail addresses: paul.armand@xlim.fr (P. Armand), francois.reynaud@xlim.fr (F. Reynaud).

0377-2217/$ - see front matter © 2008 Elsevier B.V. All rights reserved.
doi:10.1016/j.ejor.2008.02.002

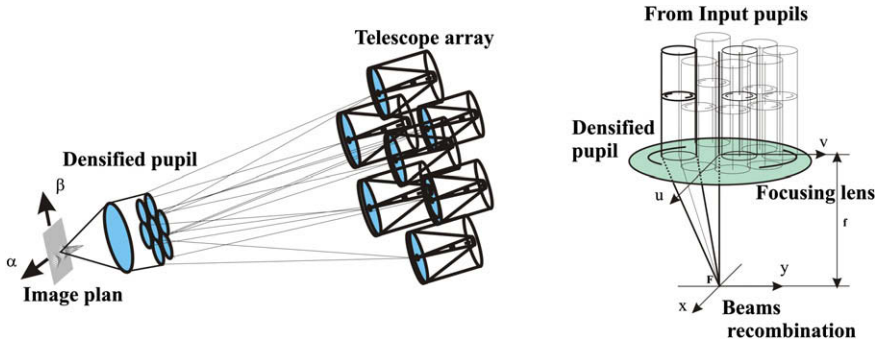

Fig. 1. Structure of a hypertelescope.

The purpose of this paper is to find the modulus of each beam and the relative positions of the output pupils to obtain high resolution and dynamic of the image. In this preliminary study, we will consider a linear array of telescopes corresponding to pupils arranged along a straight line. Applied optimization to the design of an optical instrument capable to image exoplanets has been already investigated by Kasdin et al. [3] and Vanderbei [10]. As in Vanderbei approach, we propose to formulate the design problem as a semi-infinite minimization problem. After discretization, the model problem is transformed into a constrained nonlinear minimization problem. Then, the problem is solved by using a nonlinear optimization solver.

The paper is organized as follows. In Section 2, we first present our general experimental setup, then we state the particular case of a linear array of telescopes in Section 3. The optimization model is presented in Section 4. A starting point strategy for the optimization solver is discussed in Section 5, then numerical experiments are presented in Section 6.

2. Densified pupil and point spread function

This section is focused on the optical field description in the densified pupil and to derive the corresponding point spread function.

The optical field of a monochromatic plane wave through a pupil is characterised by a modulus and a phase. We assume that all beams have the same phase (cophasing assumption). It follows that the optical field of n pupils centered at (u_k, v_k), $k = 1, \ldots, n$ and with the same diameter d is given by

$$g(u,v) = \sum_{k=1}^{n} a_k \mathbf{1}_{B_k}(u,v),$$

where a_k is the modulus of beam k and $\mathbf{1}_{B_k}$ is the characteristic function of the closed disk with center (u_k, v_k) and diameter d.

In the image plane, the optical field is the Fourier transform of the function g and is defined by

$$\hat{g}(x,y) = \iint g(u,v) \mathrm{e}^{-\frac{2i\pi}{\lambda f}(xu+yv)} \,\mathrm{d}u\,\mathrm{d}v,$$

where λ is the wave length and f is the focal length. The image plane intensity is given by the point spread function (PSF) and is defined to be the square of the modulus of $\hat{g}$. We defined the normalized PSF by

$$\Psi(x,y) = \frac{|\hat{g}(x,y)|^2}{|\hat{g}(0,0)|^2}.$$

Fig. 2 shows the graph of a normalized PSF obtained with four pupils. Our aim is to find moduli a_k and positions (u_k, v_k) such that the main central lobe is as narrow as possible, to get a high resolution, and the secondary lobes are as low as possible, to get a strong dynamic.

Let B be the closed disk with center 0 and diameter d. Let s be the surface of one pupil of diameter d. Since all pupils have the same diameter, the normalized PSF can be written as

$$\Psi(x,y) = \frac{1}{s}\left|\hat{h}(x,y)\right|^2 \frac{\left|\sum_{k=1}^{n} a_k \mathrm{e}^{-\frac{2i\pi}{\lambda f}(xu_k+yv_k)}\right|^2}{\left|\sum_{k=1}^{n} a_k\right|^2}, \tag{1}$$

where

$$\hat{h}(x,y) = \iint \mathrm{e}^{-\frac{2i\pi}{\lambda f}(xu+yv)} \mathbf{1}_B(u,v)\,\mathrm{d}u\,\mathrm{d}v,$$

is the PSF associated to only one pupil. Since the normalized PSF is homogeneous with respect to a_k, we can assume that

$$\sum_{k=1}^{n} a_k = 1. \tag{2}$$

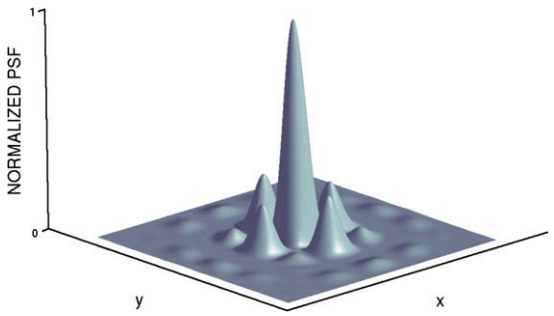

Fig. 2. Normalized PSF with four pupils.

3. Linear array of telescopes

In this first paper, we consider the particular case of a linear array of telescopes, that is $v_k = 0$ for all $k = 1, \ldots, n$ in (1). Taking (2) into account, the normalized PSF becomes

$$\Psi(x,y) = \frac{1}{s^2}|\hat{h}(x,y)|^2 \left| \sum_{k=1}^{n} a_k e^{-\frac{2i\pi}{\lambda f} x u_k} \right|^2.$$

In the right-hand side of the above formula, the term which contains the optimization parameters a_k and u_k does not depend on y. It follows that in our study we can then set y to any arbitrary value. Let us set $y = 0$. By introducing the polar coordinates $u = r\cos\theta$ and $v = r\sin\theta$, the value of $\hat{h}$ at $(x,0)$ can be written

$$\hat{h}(x,0) = \int_0^{d/2} \int_0^{2\pi} e^{-\frac{2i\pi}{\lambda f} x r \cos\theta} r \, d\theta \, dr.$$

By using the change of variable $\alpha = \frac{d}{\lambda f} x$, we can then write $\hat{h}$ as a function of α, that is

$$\hat{h}(\alpha) = \frac{2s}{\pi\alpha} J_1(\pi\alpha),$$

where J_1 is the first-order Bessel function of the first kind. The normalized PSF can then be written as a function of α and becomes

$$\Psi(\alpha) = \left| \frac{2}{\pi\alpha} J_1(\pi\alpha) \right|^2 \left| \sum_{k=1}^{n} a_k e^{-\frac{2i\pi u_k}{d}\alpha} \right|^2. \tag{3}$$

4. Optimization model

In the particular case of regularly spaced pupils, the second term in the right-hand side of (3) can be interpreted as a truncated Fourier series of some periodic function. This function can be seen as a size function to obtain a given PSF. This technique is used for the design of antenna array in telecommunication network where such a function is called an apodization function. In this specific case the parameters a_k are then the Fourier coefficients of the apodization function (see e.g., [2]). In our case, the inconvenience of this approach is that the values of dynamic and resolution do not depend straightforwardly on the choice of the apodization function, so that it is not clear how to choose such a function to get optimal a_k. Moreover, it is not sure that the choice of a regular spacing of the pupils leads to the best solution. We do not go further along this approach.

We formulate the problem as follows. We must find the moduli a_k and the positions u_k for which the PSF is as small as possible in a region close to the main central lobe. We define an interval $[\alpha_{\min}, \alpha_{\max}]$ of α values for which we want that the values $\Psi(\alpha)$ are as small as possible. It is in this interval that the main central lobe of a secondary source of light could be detected. We call it the *clean field of view* (CLF). Our optimization model is then

$$\begin{aligned} \text{minimize} \quad & \max\{\Psi(\alpha) : \alpha_{\min} \leqslant \alpha \leqslant \alpha_{\max}\}, \\ \text{subject to} \quad & u_{k+1} - u_k \geqslant d, \quad \text{for } k = 1, \ldots, n-1, \\ & \sum_{k=1}^{n} a_k = 1, \\ & a_k \geqslant 0, \quad \text{for } k = 1, \ldots, n. \end{aligned} \tag{4}$$

The first constraint is those of non overlapping of the pupils and the second is the normalization constraint. To transform the problem into a computational form, by using (3) we rewrite (4) as

$$\begin{aligned} \text{minimize} \quad & t, \\ \text{subject to} \quad & \left| \frac{J_1(\pi\alpha)}{\alpha} \sum_{k=1}^{n} a_k e^{-\frac{2i\pi u_k}{d}\alpha} \right| \leqslant t, \quad \alpha_{\min} \leqslant \alpha \leqslant \alpha_{\max}, \\ & u_{k+1} - u_k \geqslant d, \quad \text{for } k = 1, \ldots, n-1, \\ & \sum_{k=1}^{n} a_k = 1, \\ & a_k \geqslant 0, \quad \text{for } k = 1, \ldots, n. \end{aligned} \tag{5}$$

This is a semi-infinite nonlinear optimization problem. There is only a finite number of optimization variables, but an infinite number of constraints. To solve the problem we simply use a discretization method.

Suppose now that there is an even number $n = 2m$ of pupils. The case of an odd number could be considered similarly. We assume also that the pupils are symmetrically placed around zero. By discretizing the interval $[\alpha_{\min}, \alpha_{\max}]$ in (5) with q points uniformly spaced, the optimization model becomes

$$\begin{aligned} \text{minimize} \quad & t, \\ \text{subject to} \quad & -t \leqslant \frac{J_1(\pi\alpha_j)}{\alpha_j} \sum_{k=1}^{m} a_k \cos\left(\frac{2\pi}{d} u_k \alpha_j\right) \leqslant t \\ & \text{for } j = 1, \ldots, q, \quad u_1 \geqslant \frac{d}{2}, \\ & u_{k+1} - u_k \geqslant d, \quad \text{for } k = 1, \ldots, m-1, \\ & \sum_{k=1}^{m} a_k = \frac{1}{2}, \\ & a_k \geqslant 0, \quad \text{for } k = 1, \ldots, m. \end{aligned} \tag{6}$$

This is a nonlinear optimization problem with a finite number of variables and constraints. In our experiments, the number of discretization points was set to $q = 10n$.

The solution of problem (6) requires the use of a nonlinear optimization solver. In our experiments, we used the modelling language AMPL [1] to formulate the problem. The values of the Bessel function in (6) were computed by using a routine from the GNU Scientific Library. The problem has been solved by using the open source solver IPOPT [11]. It is an optimization package designed to com-

pute local solutions of a nonlinear optimization problem of the form

$$\begin{aligned} &\text{minimize} \quad f(x), \\ &\text{subject to} \quad c_i(x) = \text{ or } \leqslant 0, \quad i = 1, \ldots, m, \end{aligned}$$

where $f : \mathbb{R}^n \to \mathbb{R}$ and $c : \mathbb{R}^n \to \mathbb{R}^m$ are objective and constrained functions. It uses an interior-point algorithm to solve the first-order optimality conditions of the minimization problem. Note that other approaches, such as sequential quadratic programming or augmented Lagrangian algorithm, could also be used to solve the problem. But here, an interior-point method is well adapted because the problem possesses a great number of inequalities and these methods are well competitive in such a case.

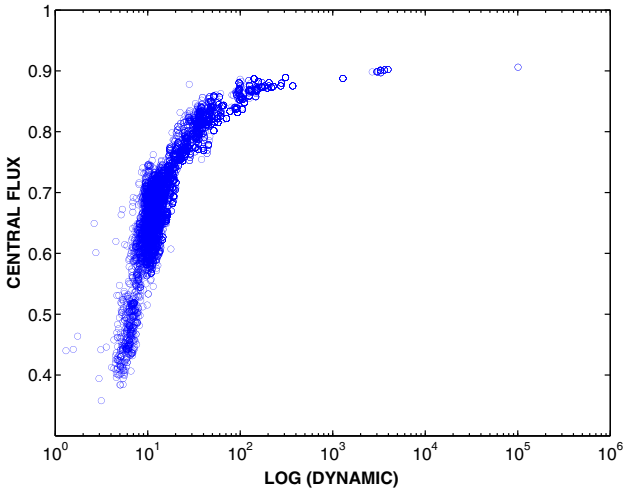

Fig. 3. Comparison of 10^4 solutions of problem (6) with different starting points.

5. Starting point strategy

A difficulty when solving problem (6) is to avoid to be trapped by a locally optimal point which is not a global minimizer, a common situation which is hard to deal within nonlinear optimization. To cope with this difficulty we considered to solve several occurrences of the same problem but with a random starting point for the solver. We solved an instance of problem (6) with eight pupils ($m = 4$), $d = 1$, $\alpha_{\min} = 0.25$ and $\alpha_{\max} = 0.75$. The starting points were chosen following a uniform distribution such that $\frac{7}{2}d \leqslant u_4 \leqslant 14d$ and that the pupils do not overlap. To compare the computed solutions, we define two measures. The first one is the optimization criterion, which we call the *dynamic* of a configuration. It is defined as the inverse of the maximum value of the normalized PSF over the CLF, that is

$$D = \frac{1}{\max\{\Psi(\alpha) : \alpha_{\min} \leqslant \alpha \leqslant \alpha_{\max}\}}.$$

The second measure is on the relative amount of energy that lands in the interval $[0, \alpha_{\min}]$. We define the *central flux* by

$$F = \frac{\int_0^{\alpha_{\min}} \Psi(\alpha)\mathrm{d}\alpha}{\int_0^{\infty} \Psi(\alpha)\mathrm{d}\alpha}.$$

Fig. 3 shows the values of dynamic and central flux for a sample of 10^4 occurrences of minimization procedures. It is clear that there is a best solution amongst all the others. Fig. 4 gives a representation of this optimal solution and the graph of the corresponding normalized PSF in linear and logarithmic scales. Table 1 reports the optimal values of a_k and u_k. Note that for the presentation of the numerical values and since the normalized PSF is homogeneous to a_k, the values of a_k are renormalized such that the

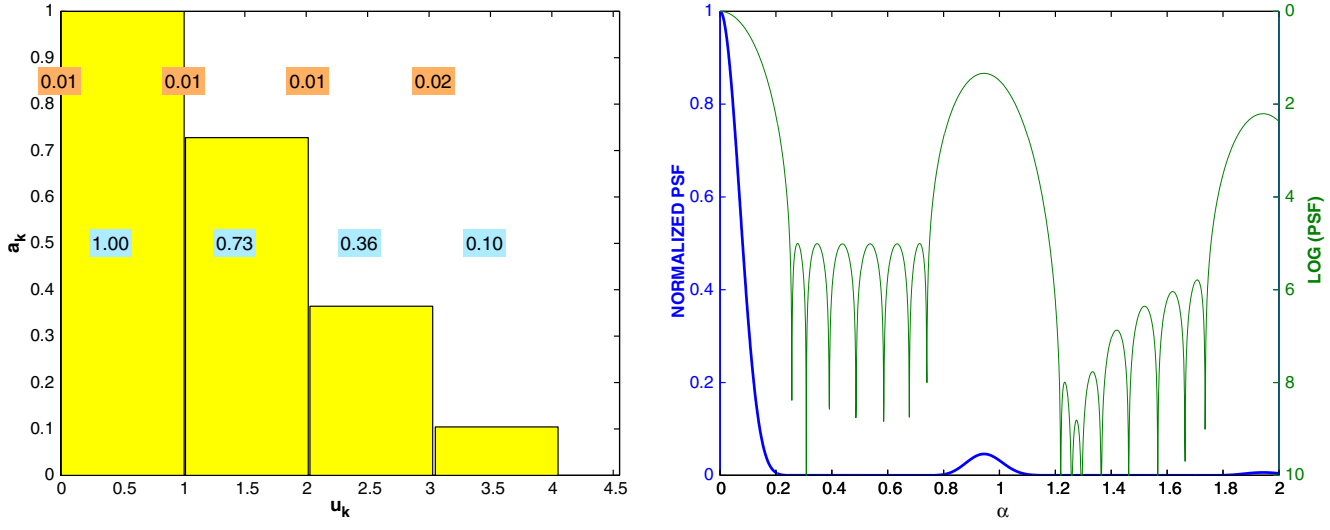

Fig. 4. Best solution found amongst 10^4 occurrences of problem (6) when $[\alpha_{\min}, \alpha_{\max}] = [0.25, 0.75]$. On the left figure, each rectangle represents the modulus of a pupil, the numbers on top are the distance between two pupils, the numbers in the middle are the coefficients a_k. The right figure shows the graph of the normalized PSF in linear and logarithmic scale.

Table 1
Optimal values for the best solution

k	a_k	u_k	$u_k - u_{k-1}$
1	1.0000	0.5054	1.0108
2	0.7277	1.5167	1.0113
3	0.3644	2.5299	1.0132
4	0.1044	3.5510	1.0211

The value u_0 is set to the position of the pupil symmetric to the first one with respect to zero.

greatest component (generally a_1) is equal to one. Note also that the accuracy of the optimal values a_k and u_k depends on the convergence tolerance of the optimization solver. In our experiments, we used a convergence tolerance of 10^{-10} (`tol` value in IPOPT package). This allows to obtain an absolute precision of at least 10^{-8} on the optimal values of a_k and u_k.

It is important to note that the optimal positions of the pupils are nearly periodic. By analysing some other similar experiments, we always observed that the best solution shows a quasi-periodic positioning of the pupils. We found that the initial-positions defined by

$$u_k = \left(k - \frac{1}{2}\right)\frac{d}{\alpha_{\min} + \alpha_{\max}}, \quad k = 1, \ldots, m, \tag{7}$$

give a fairly good estimate of the optimal positions.

Our starting point strategy is as follows. Problem (6) is solved with the variables u_k fixed to the values defined by (7). Note that in that case, (6) is reduced to a linear programming problem and thus the global optimality of the computed solution can be guaranteed. Then, starting from these optimal values, the solver is rerun to solve (6) with respect to the whole set of variables. This strategy works fine in practice. On one hand, IPOPT is able to compute the optimal solution in some tens of iterations. On the other hand, the computed solution seems to be the global minimum, though we are not able to prove it, except in some trivial cases with two or three pupils.

6. Numerical experiments

We first analyse the effect of the choice of the CLF interval on an optimal configuration. Let us define a third measure of the quality of a given configuration. Let $\rho \in [0, 1]$ be such that

$$\Psi(\rho) = \min\left\{\alpha \in [0,1] : \Psi(\alpha) = \frac{1}{2}\right\}.$$

This is the width of the PSF curve at half height of the main central lobe. The *number of resels* is the ratio

$$R = \frac{\alpha_{\max} - \alpha_{\min}}{\rho}.$$

This is the number of resolved elements in the clean field of view interval.

Let us observe the variations of the three parameters, dynamic (D), number of resels (R) and central flux (F) when the CLF interval varies. Fig. 5 (left) shows the variation of these measures for different values of the width $\Delta\alpha := \alpha_{\max} - \alpha_{\min}$. The experiments correspond to a configuration with $d = 1$ and $n = 8$. The numerical values are reported in Table 2a.

We can observe that the number of resels increases with $\Delta\alpha$, while the dynamic goes to smaller values. The variation of the central flux is not really significant. Figs. 6 and 7 show the solution of the two extreme values in Table 2a.

Fig. 5 (right) shows the variation of D, R and F for a fixed width ($\Delta\alpha = 0.4$), but for different values of $\alpha_{\min}$. The corresponding numerical values are reported in Table 2b. Figs. 8 and 9 show the resulting optimal solution of the two extreme values in Table 2b. We can observe that good values of dynamic and central flux are obtained when $\alpha_{\min}$ is far away from zero. On the contrary, the number of

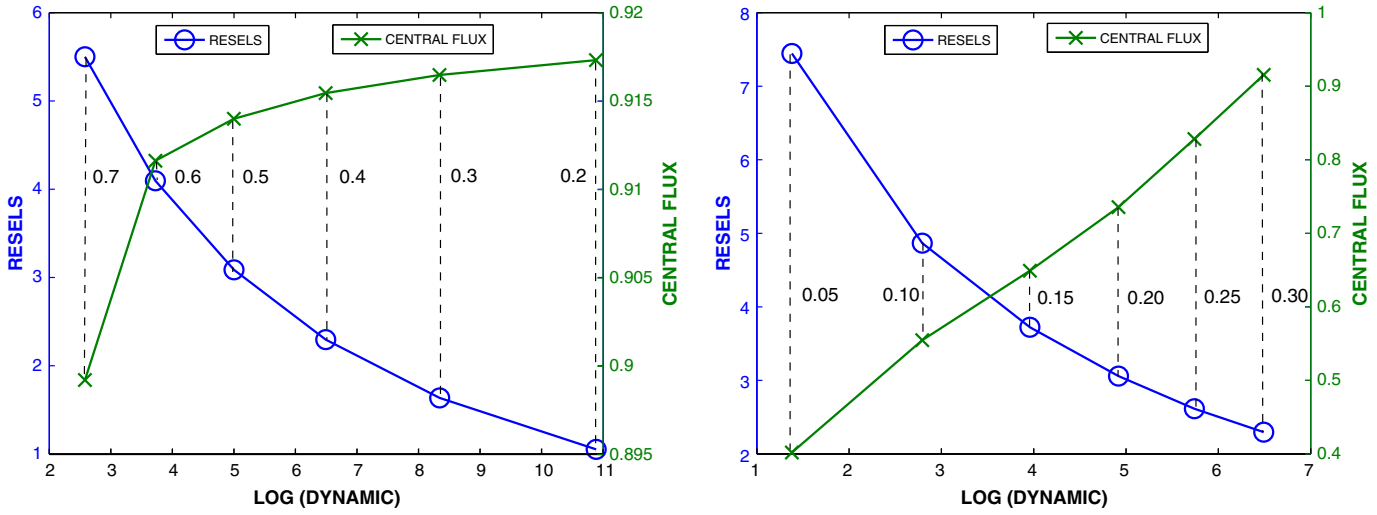

Fig. 5. Values of dynamic, central flux and number of resels according to a variation of $\Delta\alpha$ (on left), of $\alpha_{\min}$ but with $\Delta\alpha = 0.4$ (on right).

Table 2
Values of dynamic, number of resels and central flux according to the variation of $\Delta\alpha$ (a) and α_{min} with $\Delta\alpha = 0.4$ (b)

α_{min}	α_{max}	$\Delta\alpha$	D	R	F
a					
0.40	0.60	0.2	7.7e10	1.1	0.917
0.35	0.65	0.3	2.2e8	1.6	0.916
0.30	0.70	0.4	3.1e6	2.3	0.915
0.25	0.75	0.5	1.0e5	3.1	0.914
0.20	0.80	0.6	5.3e3	4.1	0.912
0.15	0.85	0.7	3.8e2	5.5	0.899

α_{min}	α_{max}	D	R	F
b				
0.05	0.45	2.4e1	7.4	0.402
0.10	0.50	6.2e2	4.9	0.555
0.15	0.55	9.1e3	3.7	0.649
0.20	0.60	8.3e4	3.1	0.736
0.25	0.65	5.5e5	2.6	0.828
0.30	0.70	3.1e6	2.3	0.915

resels increases when α_{min} goes closer to zero, which comes from the fact that the main central lobe narrows.

We study the effect of the number of pupils on an optimal configuration. We first choose a given CLF interval. Problem (6) is solved with $d = 1$, $\alpha_{min} = 0.25$ and $\alpha_{max} = 0.75$ and for different number of pupils ($n = 4, 8, 16,$ and 24). The results are reported in Table 3a. We can see that the dynamic can go to very large values when the number of pupils increases. The number of resels increases slowly because the CLF interval is constant and the main central lobe becomes slightly narrower. The values reported in Table 3b are obtained by choosing a CLF interval such that the value of dynamic is around 10^6. We can observe that both the number of resels and the central flux increase. We can also observe that the number of resels is approximately half the number of pupils. Figs. 10 and 11 show the PSF for 24 pupils.

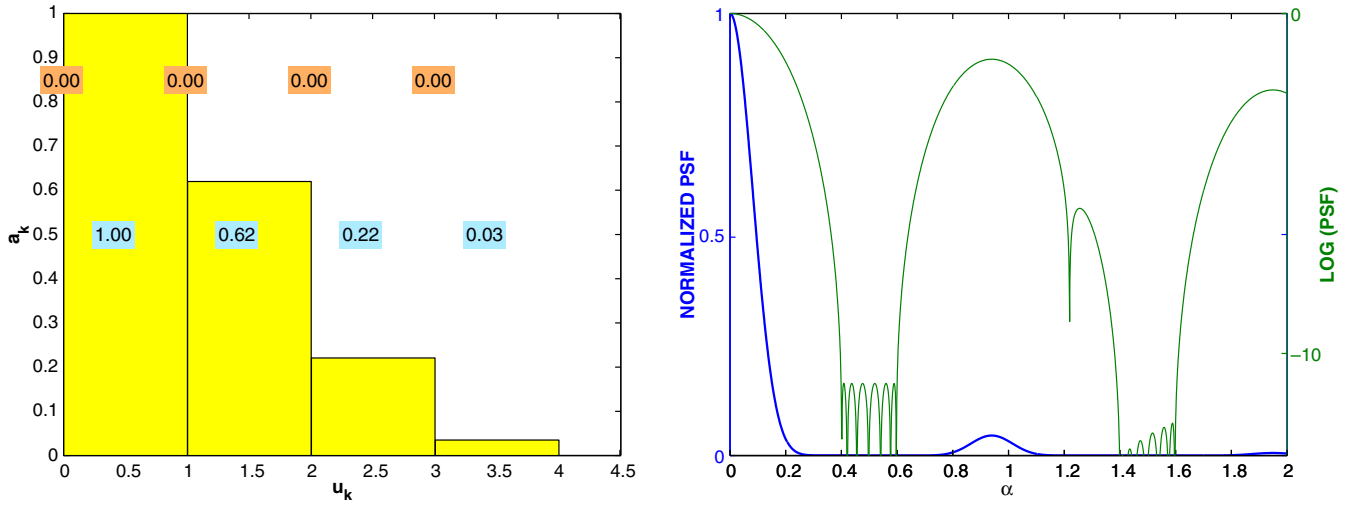

Fig. 6. Optimal solution for $[\alpha_{min}, \alpha_{max}] = [0.4, 0.6]$.

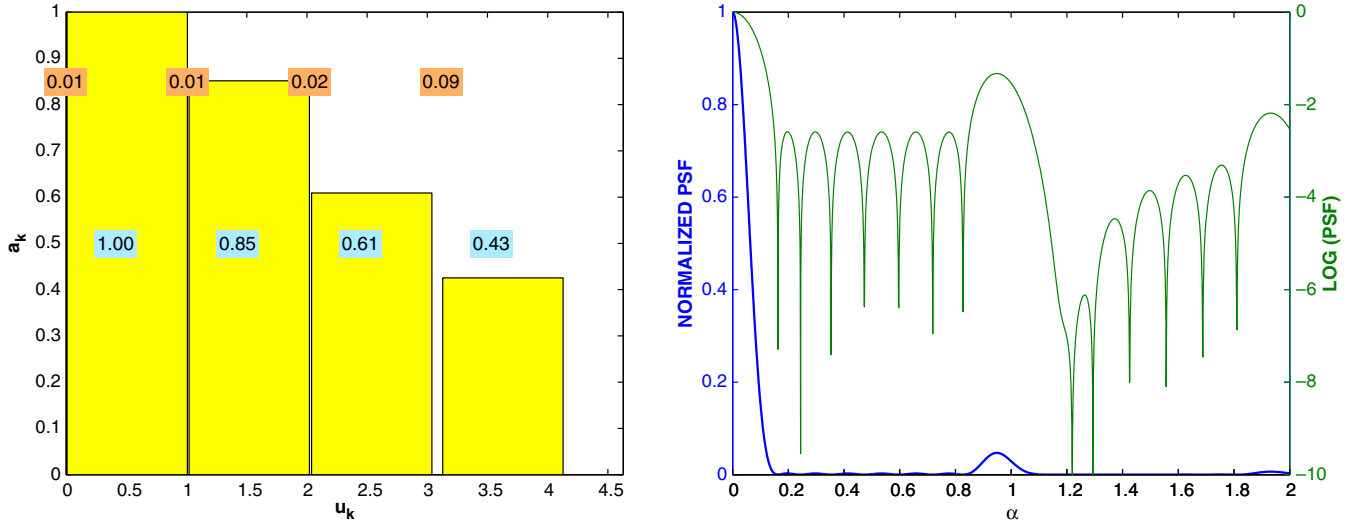

Fig. 7. Optimal solution for $[\alpha_{min}, \alpha_{max}] = [0.15, 0.85]$.

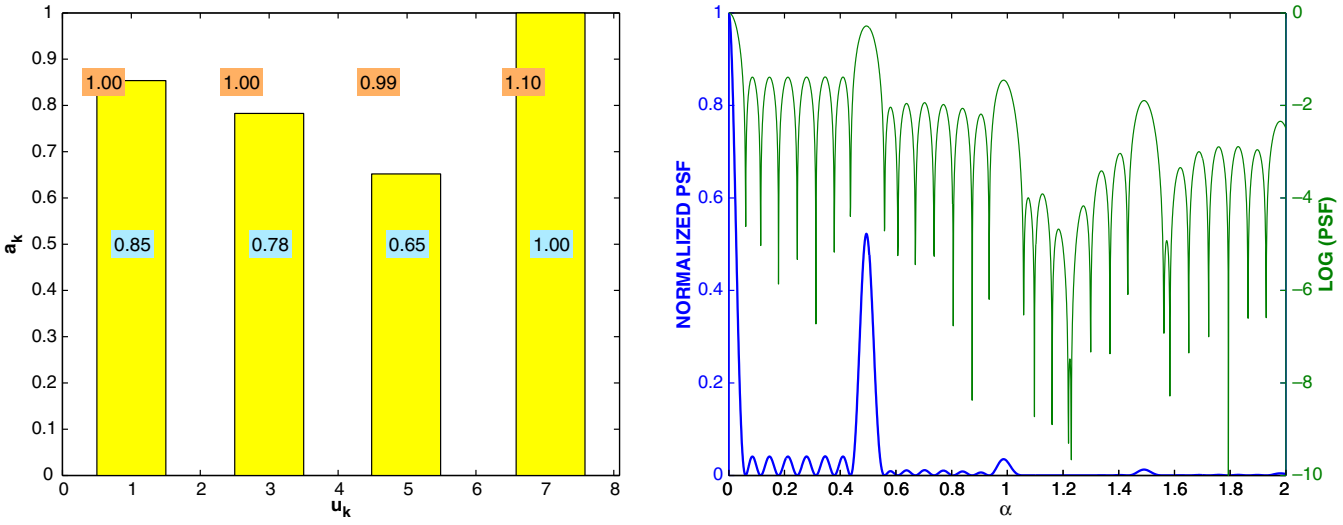

Fig. 8. Optimal solution for $[\alpha_{\min}, \alpha_{\max}] = [0.05, 0.45]$.

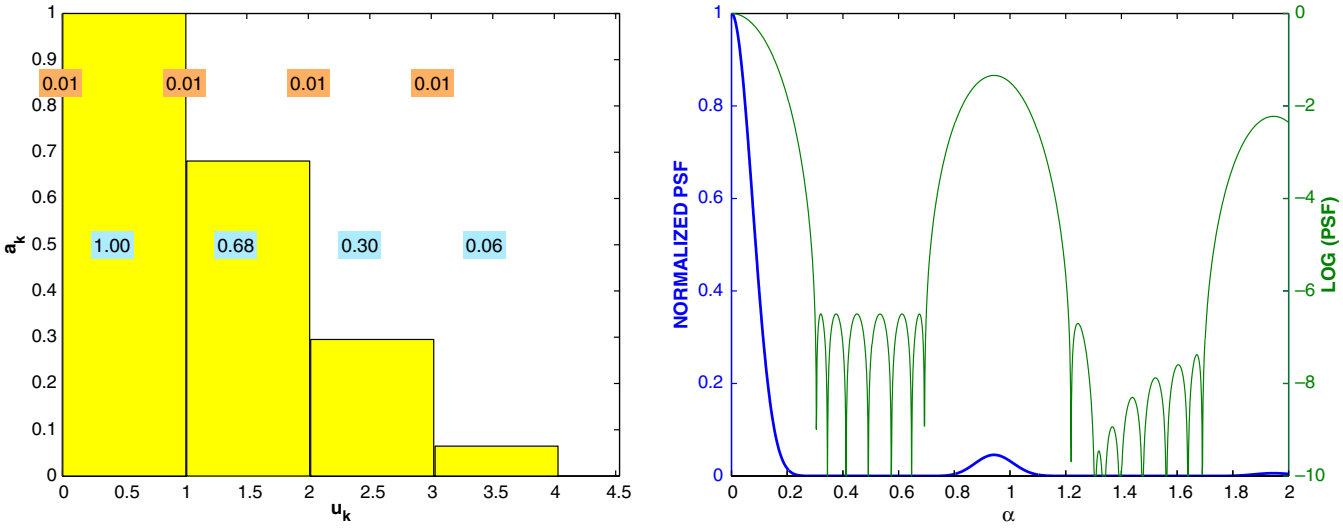

Fig. 9. Optimal solution for $[\alpha_{\min}, \alpha_{\max}] = [0.3, 0.7]$.

Table 3
Values of dynamic, number of resels and central flux according to a variation of the number of pupils

n	D	R	F
(a) $[\alpha_{\min}, \alpha_{\max}] = [0.25, 0.75]$			
4	9.1e1	2.1	0.8728
8	1.0e5	3.1	0.9140
16	1.3e11	4.4	0.9241
24	5.9e16	5.4	0.9286
(b) $D \simeq 10^6$			
4	5.9e5	0.4	0.5623
8	9.1e5	2.5	0.8734
16	1.0e6	7.7	0.7317
24	5.9e5	13.5	0.8562

We end this section by studying the sensitivity of an optimal configuration. We would like to show how some small perturbations on the optimal values of u_k and/or a_k have some effect on the measures of quality D, R and F. Starting from the optimal configuration with 8 pupils and a CLF interval equals to $[0.25, 0.75]$ (see Table 1, Fig. 4 and Table 2(a) for optimal values), we computed the PSF function and the corresponding three measures D, R and F for perturbed values a'_k and u'_k such that for $k = 1, \ldots, m$

$$a'_k = a_k(1 + t_k) \quad \text{and}$$
$$u'_k - u'_{k-1} = \max\{1, (u_k - u_{k-1})(1 + t'_k)\},$$

where t_k and t'_k are some random numbers following a uniform distribution on $[-\tau, \tau]$. The same perturbation was applied to the second half of pupils symmetric to zero. We performed a hundred of experiments with $\tau = 10^{-3}$ and with $\tau = 10^{-2}$. To compare the solutions, we considered only the worse case, that is the configurations which return the smallest value for the three measures D,

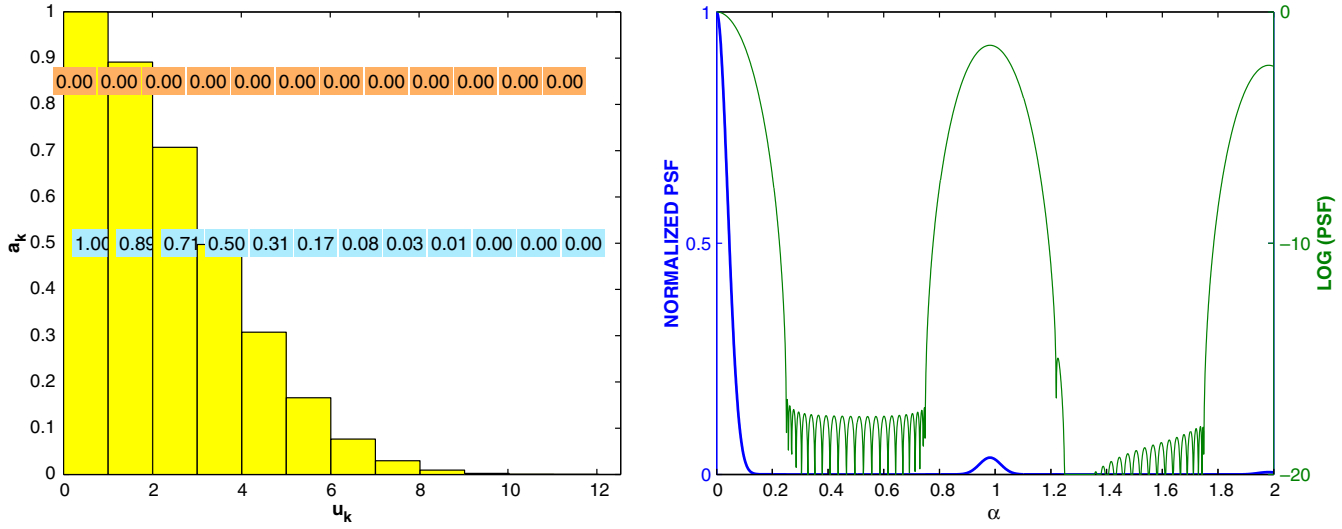

Fig. 10. Optimal solution for 24 pupils and $[\alpha_{\min}, \alpha_{\max}] = [0.25, 0.75]$.

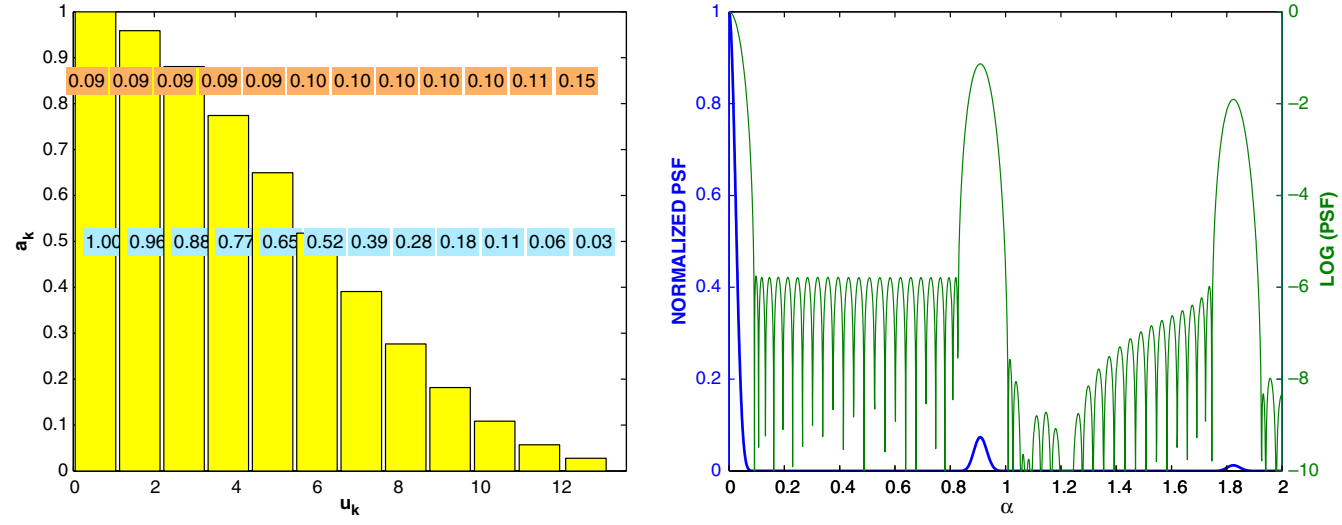

Fig. 11. Optimal solution for 24 pupils and $[\alpha_{\min}, \alpha_{\max}] = [0.09, 0.83]$.

R and F. The results are reported in Table 4. For each value of τ, three kinds of perturbation are done: beam moduli only, positions only, both moduli and positions. We observe first that only the dynamic (D) is sensitive to perturbation, the number of resels (R) and the central flux (F) are not changed or are changed very slightly. We also note that the dynamic is more sensitive to a perturbation of positions than of beam moduli. A perturbation of 1% of the position implies a decrease of a factor 10 in dynamic. Fig. 12 shows the normalized PSF with perturbed optimal parameters.

Table 4
Values of dynamic, number of resels and central flux according to a perturbation of a_k and/or u_k with 8 pupils and CLF $= [0.25, 0.75]$

τ	Perturbation	D	R	F
10^{-3}	Moduli	8.0e4	3.085	0.914
	Positions	7.0e4	3.084	0.914
	Both	6.6e4	3.083	0.913
10^{-2}	Moduli	2.2e4	3.074	0.914
	Positions	8.9e3	3.069	0.908
	Both	9.0e3	3.068	0.908

7. Conclusion

Hypertelescopes appear to be good candidates for the next generation of high resolution and high dynamic imaging device for astronomy. The optimization of the point spread function is a crucial step to maximize the efficiency of these imaging systems. This paper has demonstrated the potential of nonlinear optimization technology to adjust the densified pupil configuration in order to address specific observation program (i.e. resolution, dynamic). As a preliminary approach, this work has been done in the context of a linear array. We plan to extend this study to a two

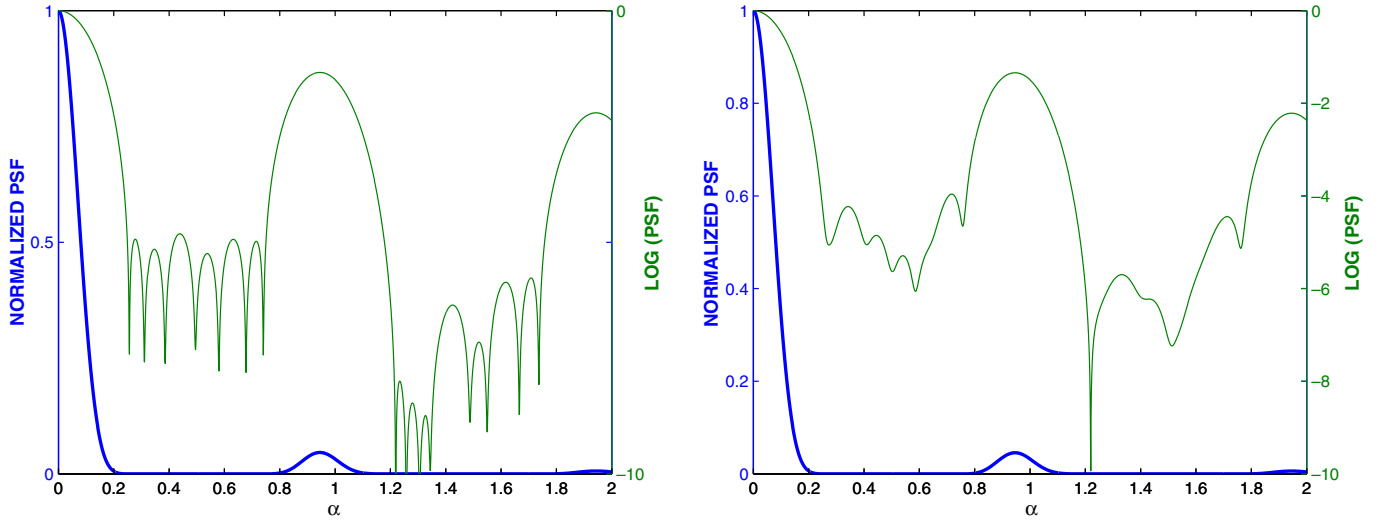

Fig. 12. Normalized PSF with perturbed optimal parameters ($\tau = 10^{-3}$ on left and $\tau = 10^{-2}$ on right). Compare with the optimal configuration shown in Fig. 4.

dimensional array and to generalize this method to the different configurations to be used with a hypertelescope.

Acknowledgement

This work is supported by the Centre National d'Étude Spatiale (CNES).

References

[1] R. Fourer, D.M. Gay, B.W. Kernighan, AMPL A Modeling Language for Mathematical Programming, second ed., Duxbury Press Brooks Cole Publishing Co., 2003.
[2] E. Hecht, Optics, second ed., Addison-Wesley Publishing Company, 1987.
[3] N.J. Kasdin, R.J. Vanderbei, D.N. Spergel, M.G. Littman, Extrasolar planet finding via optimal apodized-pupil and shaped-pupil coronagraphs, The Astrophysical Journal 582 (2003) 1147–1161.
[4] A. Labeyrie, Resolved imaging of extra-solar planets with future 10–100 km optical interferometric arrays, Astronomy & Astrophysics 118 (1996) 517–524.
[5] A. Labeyrie, S.G. Lipson, P. Nisenson, An Introduction to Optical Stellar Interferometry, Cambridge University Press, 2006.
[6] P.R. Lawson, Selected papers on long baseline stellar interferometry, vol. MS 139, Spie Milestone Series, second ed., 1997.
[7] M. Martínez-Corrala, P. Andrésa, J. Ojeda-Castañedab, G. Saavedraa, Tunable axial superresolution by annular binary filters. Application to confocal microscopy, Optics Communications 119 (1995) 491–498.
[8] F. Reynaud, L. Delage, Proposal for a temporal version of a hypertelescope, Astronomy & Astrophysics 465 (2007) 1093–1097.
[9] F. Vakili, E. Aristidi, L. Abe, B. Lopez, Interferometric remapped array nulling, Astronomy & Astrophysics 421 (2004) 147–156.
[10] R.J. Vanderbei, Extreme optics and the search for Earth-like planets, Mathematical Programming 112 (2008) 255–272.
[11] A. Wächter, L.T. Biegler, On the implementation of an interior-point filter line-search algorithm for large-scale nonlinear programming, Mathematical Programming 106 (2006) 25–57.